ESTIMATING ECONOMIC LOSSES OF MID-RISE RC SHEAR WALL BUILDINGS IN SEDIMENTARY BASINS BY COMBINING EMPIRICAL AND SIMULATED SEISMIC HAZARD CHARACTERIZATIONS

Pouria Kourehpaz[1], Carlos Molina Hutt[1], Nasser A. Marafi[2], Jeffrey W. Berman[3], and Marc O. Eberhard[3]

[1]Department of Civil Engineering, University of British Columbia, Vancouver, BC, Canada.

[2]Risk Management Solutions, Inc., Newark, CA, USA.

[3]Department of Civil & Environmental Engineering, University of Washington, Seattle, WA, USA.

Studies of recorded ground motions and simulations have shown that deep sedimentary basins can greatly increase the intensity of earthquake ground motions within a period range of approximately 1-4 s, but the economic impacts of basin effects are uncertain. This paper estimates key economic indicators of seismic performance, expressed in terms of earthquake-induced repair costs, using empirical and simulated seismic hazard characterizations that account for the effects of basins. The methodology used is general, but the estimates are made for a series of 8- to 24-story residential reinforced concrete shear wall archetype buildings in Seattle, WA whose design neglects basin effects. All buildings are designed to comply with code-minimum requirements (i.e. reference archetypes), as well as a series of design enhancements, which include: (a) increasing design forces, (b) decreasing drift limits, and (c) a combination of these strategies. As an additional reference point, a performance-based design is also assessed. The performance of the archetype buildings is evaluated for the seismic hazard level in Seattle according to the 2018 National Seismic Hazard Model (2018 NSHM), which explicitly considers basin effects. Inclusion of basin effects results in an average threefold increase in annualized losses for all archetypes. Incorporating physics-based ground motion simulations to represent the large-magnitude Cascadia subduction interface earthquake contribution to the hazard results in a further increase of 22% relative to the 2018 NSHM. The most effective of the design strategies considered combines a 25% increase in strength with a reduction in drift limits to 1.5%.

KEYWORDS

Cascadia subduction zone, simulated ground motions, deep sedimentary basin effects, reinforced concrete shear walls, earthquake-induced losses.

INTRODUCTION

The Pacific Northwest has the potential to experience large-magnitude earthquakes generated by the Cascadia Subduction Zone (CSZ), which is located approximately 100 km from the city of Seattle, WA. Furthermore, the city lies above a deep sedimentary basin, which can amplify the intensity of earthquake ground motions (Choi et al., 2005; Marafi et al., 2017; Morikawa and Fujiwara, 2013). Current seismic design provisions in the US, i.e. ASCE 7-16 (ASCE, 2016), were developed according to the 2014 National Seismic Hazard Model (NSHM) (Petersen et al., 2014), which neglects basin effects. While future earthquake design provisions are likely to account for basin amplification, the economic consequences of accounting for these effects are uncertain.

Reinforced Concrete (RC) shear walls are commonly used in the western United States as the seismic force-resisting system in mid- to high-rise residential buildings (Eberhard and Meigs, 1995; Marafi et al., 2019a). Recent earthquakes, including the 2010 Maule earthquake (Chile) and the 2011 Christchurch earthquake (New Zealand), have demonstrated that modern RC shear wall buildings generally behave well in terms of life safety (Ji et al., 2017, 2018). However, due to significant damage levels (Goretti et al., 2018), post-earthquake repair of these buildings is costly and time consuming, leading to a long-lasting loss of occupancy and a slow recovery of the community.

In this paper, we study the anticipated seismic performance, expressed in terms of earthquake-induced repair costs, of seven design variations of a range of 8- to 24-story residential RC shear wall buildings in Seattle. A reference archetype, designed to comply with minimum ASCE 7-16 (ASCE, 2016) code-prescriptive requirements, is evaluated. Additionally, a series of code-prescriptive design enhancements, five in total, are also studied. The enhancements

included: (a) increasing design forces, (b) decreasing drift limits, and (c) a combination of these strategies. Lastly, a performance-based design approach that is typically used for buildings in Seattle that exceed 73.2 m (240 ft) (City of Seattle Department of Planning and Developments, 2015) is also evaluated. The archetype buildings were designed by Marafi et al. (2020a) to quantify the impact of basin amplification on collapse risk and to devise simple design strategies to satisfy the 1% in 50-year collapse risk target of modern building codes when basin effects are considered. The nonlinear response history analyses of the archetype buildings have been published in other papers (Marafi et al. 2020a, 2020b). The novelty in this paper lies in the assessment of the earthquake impacts, expressed in terms of economic losses, which can be used to inform planners and policymakers of underlying risks, and the engineering design community of the tradeoffs of adopting different design strategies.

The performance of the archetype buildings was evaluated for the seismic hazard level in Seattle according to the 2014 NSHM, which neglects the effects of basins, as well as the 2018 NSHM, which explicitly considers basin effects (Petersen et al., 2020). The archetype buildings were also subjected to 30 simulated scenarios of a magnitude-9 (M9) CSZ interface earthquake, generated by Frankel et al. (2018). These simulated ground motions were used to devise a hybrid seismic hazard model, which is based on the 2018 NSHM, but utilizes physics-based simulations to represent the large interface earthquake portion of the hazard and empirical relationships for all other earthquake sources (crustal and intraslab).

Numerous studies have quantified the earthquake-induced economic losses of modern and existing frame buildings. For instance, Hwang and Lignos (2017) evaluated the seismic performance of modern steel moment-resisting frames, whereas Molina Hutt et al. (2016, 2019) evaluated the performance of pre-Northridge steel moment frames. The performance of modern code-conforming (Ramirez et al., 2012) and non-ductile (Baradaran Shoraka et al., 2013) RC moment frames has also been widely studied. In contrast, there are few analytical studies on the earthquake-induced repair costs of RC shear wall buildings. In addition to addressing this knowledge gap, this study quantifies the impact of basin amplification and variations in strength, stiffness, and building height on the earthquake-induced repair costs of RC shear wall buildings in Seattle.

CONSIDERING DEEP SEDIMENTARY BASINS IN STRUCTURAL DESIGN

Past studies have shown that recorded motions have spectral accelerations that are larger at long periods for locations in deep sedimentary basins than for locations outside the basins with similar site-to-source distance (Bozorgnia et al., 2014; Choi et al., 2005; Marafi et al., 2017; Morikawa and Fujiwara, 2013). The effects of deep sedimentary basins on ground-motion characteristics have also been observed in physics-based simulations of earthquake ground motions (Aagaard et al., 2010; Frankel et al., 2018; Graves et al., 2011; Moschetti et al., 2017; Wirth et al., 2018). In the United States, currently enforced seismic design provisions for buildings, i.e. ASCE 7-16, utilize spectral accelerations for use in design based on the 2014 NSHM, which does not consider basin amplification. In the western United States, deep basins underlie large metropolitan areas, including Seattle, as well as parts of Los Angeles, Salt Lake City, and the San Francisco Bay area. As a result, the most recent version of the national seismic hazard model, the 2018 NSHM, accounts for basin amplification on spectral accelerations in these areas, and its adoption in future design standards would result in a considerable increase in seismic design spectral accelerations.

The 2018 NSHM accounts for basin effects on spectral acceleration for all earthquake sources using basin terms adapted from the crustal earthquake ground-motion models in the NGA West2 project (Bozorgnia et al., 2014). The proxy for basin depth is the depth from the surface to a layer with a shear-wave velocity of at least 1.0 km/s or 2.5 km/s, denoted as $Z_{1.0}$ and $Z_{2.5}$, respectively. Compared to the other basins in the western United States, Seattle has the largest maximum value of $Z_{2.5}$, which is equal to 6.9 km (Stephenson et al., 2017). As a result, the spectral accelerations from the 2014 to the 2018 NSHM Uniform Hazard Spectrum (UHS) for a hazard level with a 2% probability of exceedance in 50-year is approximately 50% larger for periods in the range of 1-4 s. Increases in spectral acceleration due to basin amplification are larger at longer periods. For instance, the increase in spectral acceleration at a period of 0.2 s is only 15%, whereas for a 2.0 s period, the increase is 66% (Marafi et al., 2020a). Increases in spectral acceleration from the 2014 NSHM to the 2018 NSHM are negligible for out-of-basin sites within Western Washington State.

While the basin amplification terms used in the 2018 NSHM were developed by considering crustal earthquakes, interface earthquakes represent large contributions to the seismic hazard in Seattle, particularly at periods greater than 1 s. Comparing response spectra developed per the 2018 NSHM and M9 simulations revealed that the 2018 NSHM

underestimates the basin effect on spectral acceleration at periods longer than 1 second in the Seattle area relative to that observed in the simulations (Frankel et al., 2018; Marafi et al., 2019b). In addition, M9 simulated ground motions can be more damaging because of their longer duration and more damaging spectral shape compared to the ground motions selected to represent the 2018 National Seismic Hazard Model particularly in the period range of 0.5-3.0 s (Marafi et al., 2020b).

Recent studies have evaluated the impact of basin amplification on collapse risk. Marafi et al. (2020a) found that the collapse risk of modern RC shear wall buildings in Seattle would increase from 0.5% to 1.8% in 50-years when basin effects are considered; whereas the target maximum is 1% in ASCE 7-16. Similarly, Molina Hutt et al. (2020) found that basin effects would increase the 50-year collapse risk of 1970s steel moment frames from 6.9% to 10.5%. The impact of basin amplification on earthquake-induced repair costs has not yet been quantified.

ARCHETYPE RC SHEAR WALL BUILDINGS

Marafi et al. (2020a) studied the seismic performance of 8-, 12-, 16-, 20-, and 24-story modern residential RC shear wall building archetypes in Seattle (47.6°N, -122.3°W). Seven design variations were considered for all archetypes as summarized in Table 1. All buildings were designed and detailed by Marafi et al. (2020a) as special RC shear walls, per ACI 318-14 (2014) requirements, with a seismic force-reduction factor (R) of 6, following a modal response spectrum analysis (MRSA) procedure. The reference (REF) archetypes were designed to barely meet the minimum code-prescriptive requirements of ASCE 7-16, with a 2% maximum allowable seismic drift, and a 1.0 flexural demand-to-capacity ratio at the ground floor. To evaluate the impacts of adopting various design strategies, the REF archetypes were re-designed with an increase in design lateral loads of 25% and 50% (denoted as S25% and S50%, respectively). Additionally, the REF archetypes were re-designed with a reduction in drift limits from 2% to 1.5% and 1.25% (denoted as DL1.5% and DL1.25%, respectively). Lastly, the REF archetypes were re-designed by combining a 25% increase in design lateral loads and a reduction in drift limits to 1.5% (S25%+DL1.5%). In this study, archetypes that were designed with lower drift limits (i.e., DL1.5% and DL1.25%) had similar seismic design strengths to the base archetype because the code design strength (C_s) was computed using the upper limit on the design period, $C_u T_a$ (per ASCE 7-16). All archetypes were in the period range of the design spectrum where spectral accelerations are inversely proportional to the fundamental period of the structure. As a result, increases in stiffness also resulted in an increase in seismic demand as quantified by the Conditional Mean Spectrum (CMS). For example, for the 16-story archetypes, the 2475-year return spectral acceleration increased by 31% and 53% relative to the REF archetype for the DL1.5% and the DL1.25% design strategies, respectively.

In addition to the code-prescriptive designs, one additional design strategy followed a performance-based approach (PBD), which included nonlinear analysis to check the strain, force, and drift limits of the Tall Building Initiative (TBI) guidelines (PEER, 2017) as outlined in Seattle's Director's Rule 5 (City of Seattle Department of Planning and Developments, 2015). The reinforcing and size of the PBD walls were modified until the stress, strain and force PBD limits were met. These PBD buildings were initially designed using the ASCE 7-16 design spectra, but the strength was then modified to meet the PBD checks because the seismic hazard (i.e., nonlinear analysis using CMS motions) included basin effects, which are not considered in ASCE 7-16 code-minimum archetypes.

Table 1. Design strategies of the residential RC shear wall archetype buildings.

Design Strategy	Description
REF	Reference archetype designed per ASCE 7-16 (2% drift limit)
S25%	REF archetype redesigned with 25% increase in design lateral loads
S50%	REF archetype redesigned with 50% increase in design lateral loads
DL1.5%	REF archetype redesigned to meet 1.5% drift limit
DL1.25%	REF archetype redesigned to meet 1.25% drift limit
S25%+DL1.5%	REF archetype redesigned with 25% increase in design lateral loads and 1.5% drift limit
PBD	Performance-Based Design

In the analyses, the concrete compressive strength for the RC shear walls was assumed to be 55.2 MPa (8 ksi) and steel reinforcing had a nominal yield strength of 414 MPa (60 ksi). For all archetypes, the floor dimensions were 48.8 m long by 48.8 m wide (160 ft x 160 ft) in basement levels, and 30.5 m long by 30.5 m wide (100 ft x 100 ft) above grade (See Figure 1a), which is a typical size for mid-rise to tall buildings in Seattle All archetypes had four basement

levels except the 8-story archetypes, which only had three levels below grade. The height of all the stories was 3.05 m (10 ft). For all archetypes, the lateral force-resisting system consisted of a symmetrical central core made up of two C-shaped walls, coupled in one direction and uncoupled in the other. Steel reinforcing bars were distributed evenly to confine the entire core, which is typical in practice in Seattle (SEAW Earthquake Engineering Committee, personal communication, 2018). In addition, all archetypes had three, 9.15-m (30-ft) bays of slab-column gravity framing in each orthogonal direction around the building perimeter.

It is expected that increasing strength and stiffness of the archetype would improve performance; however, such design changes would consequently impact architectural layout and material quantities. Figure 1 depicts the average (across all stories) RC shear wall gross area and longitudinal steel reinforcement areas normalized by the total floor area. These metrics highlight how the design variations, in nearly all of 8- to 24-story archetypes, utilize a larger volume of concrete than the REF archetype. For all building heights, the S50% design strategy results in the largest increase in RC shear wall as compared to other strategies and even more notable increases occur with building height. For instance, the increase in RC shear wall area for the 8-story S50% relative to REF archetype is 39%, whereas for the 24-story, it is 98%. The amount of longitudinal steel in all archetypes fluctuates across designs. However, for all building heights, the S50% archetype utilizes the highest percentage of longitudinal steel. For example, the 16-story S50% design uses 47% more steel than the 16-story REF archetype. In contrast, stiffer archetypes (e.g., DL1.25%) resulted in lower steel tonnages because these archetypes had steel bars placed further apart (i.e., larger moment arms) which reduced the overall steel area to achieve a similar design strength from the REF archetype. Additional details of the RC shear wall building designs can be found in Marafi et al. (2020a).

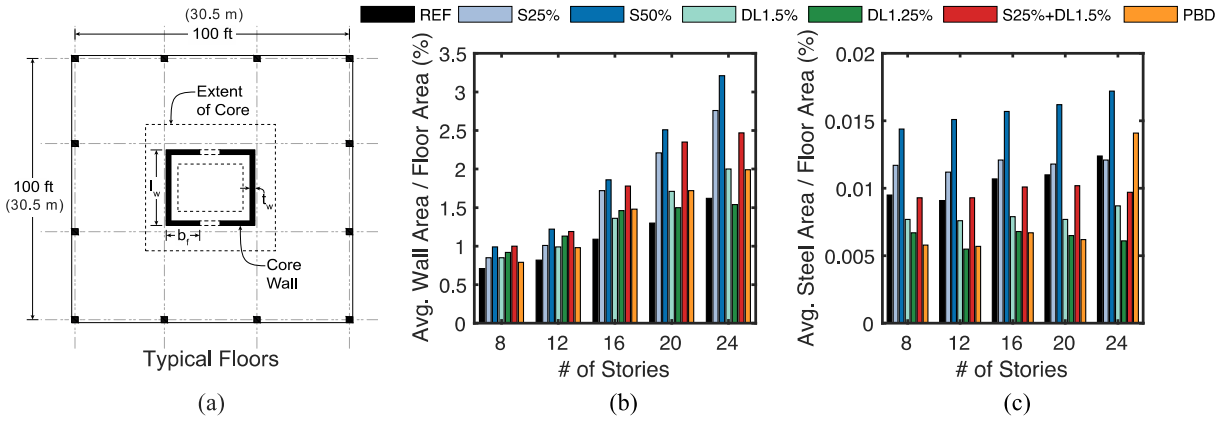

Figure 1. (a) Typical floor plan view, (b) average RC shear wall area as percentage of floor area, and (c) average longitudinal steel reinforcement area as percentage of floor area for different design strategies of 8- to 24-story buildings.

SEISMIC PERFORMANCE ASSESSMENT METHODOLOGY

Seismic Hazard and Ground Motions

The seismic performance of each archetype building was evaluated using a multiple stripe analysis (MSA) procedure (Jalayer and Cornell, 2009) consistent with that outlined in Marafi et al. (2020a). In MSA, structural assessments are performed at a series of ground motion intensities spanning from high to low probability of exceedance. The lower- and upper-bound intensity measure levels considered cover a range from negligible damage to complete loss. Nonlinear dynamic analyses were conducted with ground motion suites representative of each intensity level. The analysis results were then linked back to probabilistic seismic hazard data, which enables calculating a range of risk metrics, such as annualized losses.

The intensity measure used in the MSA was the spectral acceleration at the fundamental period (T_1) of each archetype building. The MSA utilized median spectral acceleration over all orientations (SA_{RotD50}) to permit integration with probabilistic seismic hazard data. The intensity stripes used in the MSA had return periods of 100, 475, 975, 2475, and 4975-years. A Conditional Mean Spectrum (CMS) was used to represent the expected ground motion response spectrum conditioned on the occurrence of the target spectral acceleration at the fundamental period of each archetype.

The CMS was calculated as a weighted average of the CMS for each ground-motion model and particular seismic source (e.g., Seattle fault) according to its percentage contribution to the hazard, as obtained from seismic hazard deaggregation results. For each return period, the CMS was computed using the 2014 and 2018 NSHMs (USGS, 2019) for a downtown Seattle location. At each return period, 100 ground motion records consisting of crustal, interface, and intraslab earthquakes were selected such that the ratio of each different earthquake type was proportional to its contribution to the total hazard. Ground motions were selected and scaled to match the target mean and variance in Conditional Spectra (CS) (Jayaram et al., 2011). Figure 2 shows the target CMS for the crustal, intraslab and interface earthquakes per the 2018 and 2014 NSHMs at the fundamental period of 16-story REF (T~ 3.5 s).

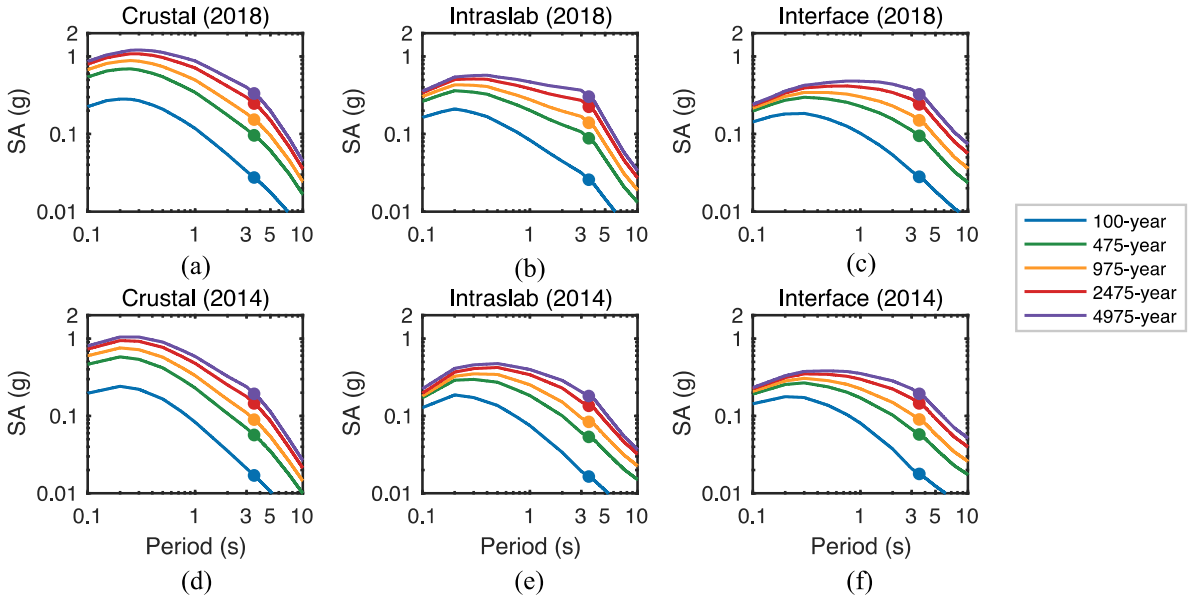

Figure 2. CMS at 3.5 s period per the 2018 NSHM for (a) crustal, (b) intraslab, (c) interface earthquakes and per the 2014 NSHM for (d) crustal, (e) intraslab, (f) interface earthquakes at different hazard levels

The archetype buildings were also subjected to 30 broadband seismograms for M9 CSZ earthquakes where each seismogram (both horizontal components) were oriented in the direction corresponding to the median spectral acceleration at the building's period (SA_{RotD50}). These earthquakes had a return period of approximately 500 years and were derived by combining synthetic seismograms from 3D finite-difference simulations (≥1 s) with finite-source stochastic synthetics (<1 s), produced by Frankel et al. (2018). The M9 simulations considered various rupture scenarios, hypocenter locations, and slip distributions and were found to match the BC Hydro ground-motion model (GMM) (Abrahamson et al., 2016) well for locations outside of the deep basins. The modelling methodology was also found to sufficiently replicate recordings from the 2010 M8.8 Maule (Chile) earthquake (Frankel, 2017) and the 2011 M9 Tohoku (Japan) earthquake (Frankel, 2013). The resulting synthetics highlight the considerable amplification of spectral accelerations, ranging from factors of 2 to 5, for periods of 1 to 10 s, for sites within the Seattle basin. Marafi et al. (2020a) showed that inside the basin the spectral accelerations of the simulated M9 CSZ ground motions at periods of 1.5 to 4 s were greater than the spectral accelerations of the ASCE 7-16 risk-targeted maximum considered earthquake (MCE_R), which has a return period of around 2000 years in Seattle.

Table 2. 2014 NSHM and 2018 NSHM SAs for intensity levels with a 975- and 2475-year return period, and mean simulated M9 ground motion SAs inside the Seattle basin.

Archetype	2014 NSHM		2018 NSHM		M9
	975-yr	2475-yr	975-yr	2475-yr	
8-Story REF (T_1 = 1.93 s)	0.23 g	0.37 g	0.32 g	0.52 g	0.34 g
12-Story REF (T_1 = 2.70 s)	0.15 g	0.25 g	0.22 g	0.36 g	0.39 g
16-Story REF (T_1 = 3.53 s)	0.11 g	0.19 g	0.16 g	0.27 g	0.48 g
20-Story REF (T_1 = 4.36 s)	0.09 g	0.15 g	0.12 g	0.21 g	0.43 g
24-Story REF (T_1 = 5.11 s)	0.07 g	0.12 g	0.10 g	0.17 g	0.44 g

Table 2 summarizes the CMS spectral acceleration, at the fundamental period of each REF archetype, using the 2014 and 2018 NSHMs for intensity levels with return periods of 975 and 2475 years. Additionally, Table 2 includes the mean spectral acceleration, at the fundamental period of each REF archetype, of the simulated M9 ground motions inside the Seattle basin. Furthermore, for taller buildings with higher fundamental periods (16-stories and above), the spectral accelerations of the M9 simulations exceed spectral accelerations of the 2475-year return period intensity level per the 2018 NSHM.

Nonlinear Simulation of Structural Response

The structural response of all archetypes was evaluated using 2D nonlinear models in OpenSees (McKenna, 2016). The axial and flexural nonlinear response of RC shear walls were captured by using displacement-based, beam-column elements with fiber sections (Marafi et al., 2020a). The nonlinear behavior of the wall was modeled using a methodology that was developed by Marafi et al. (2019a). This methodology used displacement-based, beam-column elements with lumped-plasticity fiber sections to capture the axial and flexural nonlinear responses of the core walls. The reinforcing steel response is modelled using the Steel02Fatigue material model, which uses the Menegotto and Pinto (1973) stress–strain relationship and is modified for cyclic strength degradation per Kunnath et al. (2009) recommendations. The concrete response is modelled using the Concrete02IS material model, which uses Popovics (1973) pre-peak stress-strain relationship pre-peak relationship and Yassin (1994) post-peak response. For shear, this methodology used an elastic shear model and does not account for shear-flexure interaction. Rebar buckling was accounted for by assuming that the rebar buckles and loses its entire strength once the concrete reaches its crushing strain. Marafi et al. (2019a, 2020b) provide more details of the modeling strategy. The earthquake time-history analyses were performed in the uncoupled direction of the RC shear wall buildings only, and therefore, effects of torsion and bidirectional loading on structural response were not considered. Each archetype was subjected to 100 earthquake ground motion records at each intensity level for each archetype following the 2014 and 2018 NSHMs, as well as the thirty M9 CSZ ground motion simulations.

The earthquake-induced economic loss of a structure is typically attributed to: (1) damage to the structure, which is correlated to story drift; and (2) damage of non-structural elements, which varies across different elements and it can be correlated to floor acceleration, story drift, and other measures. The results from the structural analyses are summarized in Figure 3. The figure shows the median peak story drifts and median peak floor accelerations of the 16-story REF archetype for each intensity level considered in the assessment. The figure also compares the median demands from the suite of thirty M9 simulations, where the story drifts are similar to the 2,475-year intensity level per the 2014 NSHM, and similar to the 975-year intensity level per the 2018 NSHM. As expected, the median peak story drifts increased with increasing return period, and they were larger for the 2018 NSHM than the 2014 NHSM.

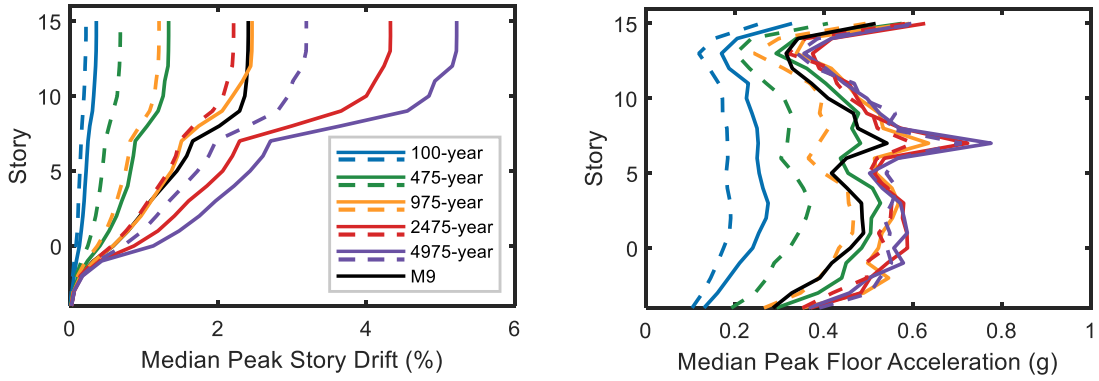

Figure 3. Median of the maximum: (a) story drift ratios and (b) floor accelerations of the 16-story REF archetype, where solid lines correspond to the 2018 NSHM and dashed lines correspond to the 2014 NSHM.

The various design strategies resulted in a significant impact on the story drift profiles. Figure 4a shows the median story drifts for a 975-year intensity using the 2014 and 2018 NSHMs for all design strategies for the 16-story archetype. The story drifts on average reduced for all design strategies compared to the REF archetype. In contrast, the design strategies did not have a significant impact on the floor accelerations. Figure 4b shows that the peak floor acceleration profile ranged from 0.50 to 0.75 g across design variations. This range in floor acceleration was either

higher or lower than the REF archetype indicating that the various design strategies did not necessarily reduce floor accelerations. Peak ground accelerations are not identical for all design strategies because each design variation has its own ground motion suite, which is conditioned on the fundamental period of the structure (unique to each design). Similar observations were found for other building heights (8-, 12-story, etc.) and intensity levels (100-year, 475-year, etc.).

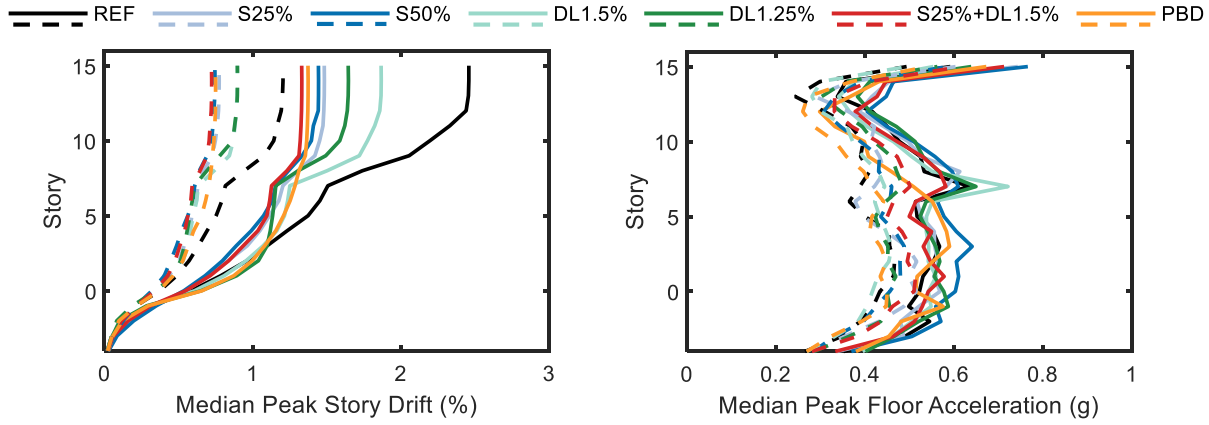

(a) (b)

Figure 4. Median of the maximum: (a) story drift ratios and (b) floor accelerations of the 16-story archetypes under the 975-year intensity level, where solid lines correspond to the 2018 NSHM and dashed lines correspond to the 2014 NSHM.

To enable the comparison of engineering demands among archetypes with a variety of heights, Figure 5 shows the engineering demands with respect to the story number normalized by the total number of stories in the archetype. The median peak story drifts and floor accelerations of REF archetypes of all heights under the 975-year intensity level are found to be similar among archetypes when subjected to ground-motions that represent the 2014 and 2018 NSHMs. In Figure 5b, the peaks in floor acceleration observed at 0.5 to 0.7 of the building height of some archetypes, e.g. 20-story NSHM 2018, are attributed to the formation of a second hinge at mid-height, because the reinforcement at the base was not continuous all the way to the top of the walls.

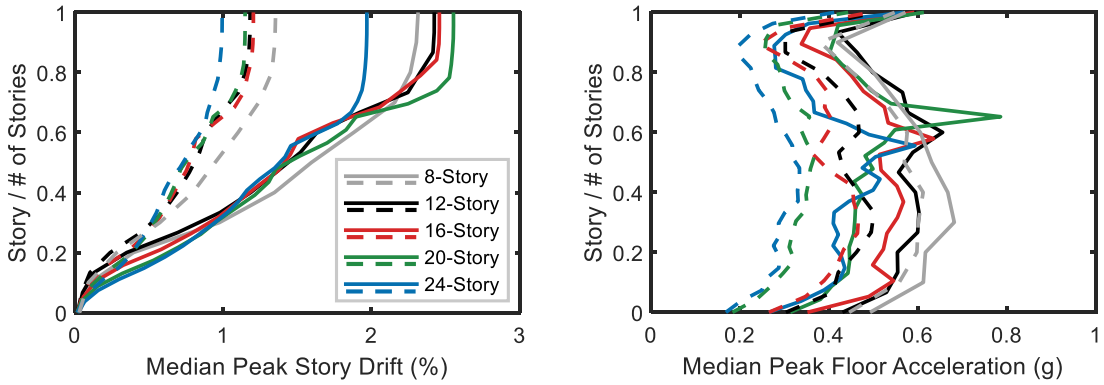

(a) (b)

Figure 5. Median of the maximum: (a) story drift ratios and (b) floor accelerations of the REF archetypes from 8 to 24 stories under the 975-year intensity level, where solid lines correspond to the 2018 NSHM and dashed lines correspond to the 2014 NSHM.

In limited instances, at high earthquake shaking intensities, dynamic instability occurred when the lateral displacement of the structure increased without bounds. Additionally, non-simulated collapse modes were also considered in the assessment. Past experimental studies showed that probability of slab-column punching shear failure with respect to slab-column rotation depends on gravity shear ratio (Hueste et al., 2009, 2007). Available experimental data for slab-columns with shear-reinforcement and a gravity shear ratio between 0.4 to 0.6, permitted describing the slab-column

rotation capacity by means of a lognormal cumulative distribution with a mean slab-column rotation of 5.9% and a dispersion of 0.12 (Dilger and Brown, 1995; Dilger and Cao, 1991; Megally and Ghali, 2000). In this study, non-simulated collapse was assumed to occur if slab-column rotation exceeded 5.9%. Hazard consistent collapse fragilities were developed for all archetypes considering both simulated and non-simulated collapses. Collapse realizations are generally driven by non-simulated collapse. For all archetypes, simulated wall failures contribute, at most, 25% of the overall conditional collapse risk at the intensity levels considered, except for the drift-controlled archetypes (DL1.5% and DL1.25%) where the simulated wall failures can contribute up to 40%. The probability of collapse at each return period was calculated by dividing the number of collapse realizations over the total number of ground motion runs. A cumulative lognormal distribution was fitted to the data using a maximum likelihood estimation procedure, as outlined by Baker (2015). Figure 6a shows the collapse fragilities of all 16-story archetype buildings considered in the assessment according to the 2018 NSHM. Because each archetype has a unique fundamental period T_1, Figure 6a shows the collapse fragilities with respect to the return period of SA_{T1} to permit a visual comparison of all collapse fragilities. It can be observed that all design strategies considered resulted in drastic reductions in the probability of collapse with respect to the REF archetype.

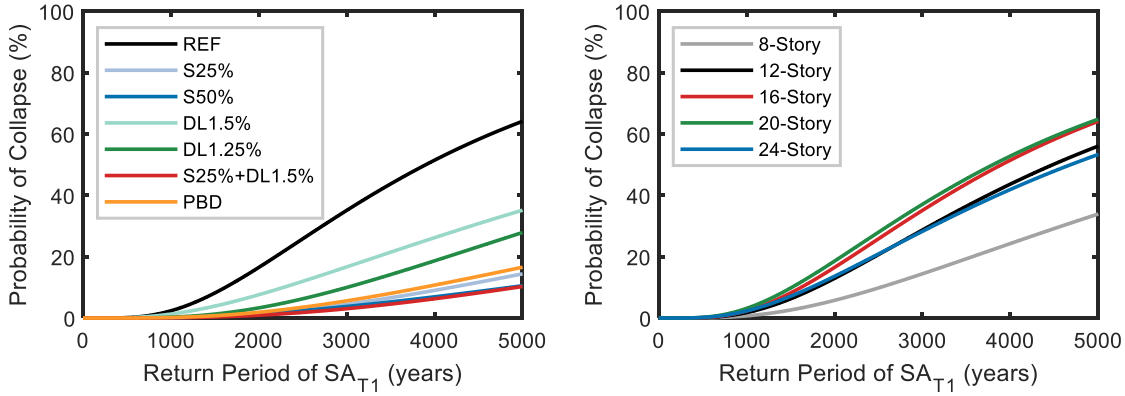

Figure 6. Collapse fragilities (a) for the 16-story RC shear wall archetypes and (b) for the REF archetypes from 8 to 24 stories per the 2018 NSHM.

Similar trends were found for the other archetypes of different heights. Figure 6b illustrates the collapse fragilities for 8- to 24-story REF archetypes per the 2018 NSHM. As seen in the Figure, the collapse probabilities conditioned on all return periods increased with building height from 8- to 20-story REF archetypes; however, there was a reduction in the collapse probabilities for the 24-story REF archetype. For example, across all REF archetypes, collapse probabilities conditioned on the 2475-year intensity level varied from 12%, for the 8-story archetype, to 35%, for the 20-story archetype and then dropped to 22% for the 24-story archetype. The design of the 24-story archetype is controlled by minimum base shear requirements, which result in a larger seismic design strength than that of the 20-story archetype. As a result, the 24-story archetype has smaller drift values, which result in fewer non-simulated collapse observations. Conditional collapse probabilities under the M9 simulations were also evaluated and varied between 0 and 17%, where the 20-story REF archetype had the highest conditional probability of collapse.

Distinct collapse fragilities were considered for all archetypes under the interface earthquakes. Considering only the interface earthquake contribution to the hazard, as opposed to all seismic sources (Figure 6a) resulted in a reduced probability of collapse for any given return period. This is because for a given spectral acceleration, the interface earthquake hazard is a fraction of total hazard. The corresponding return period for a similar spectral acceleration is greater when considering a single source than when considering all sources. Analysis of the archetype buildings with earthquake ground motions consistent with the 2014 NSHM resulted in negligible probabilities of collapse.

Loss Assessment

A risk-based assessment was carried out to calculate the average annual losses (AAL) of each archetype building. A risk-based assessment consists of the evaluation of a number of intensity-based performance assessments under a range of ground motion intensity levels, five in this study, which are then combined with the ground motion hazard

curve to provide the annual rates of exceedance of a performance measure, e.g. economic loss (NEHRP, 2011). The technical basis of this methodology was developed by the Pacific Earthquake Engineering Research (PEER) center and applies the total probability theorem to predict earthquake consequences in terms of the probability of incurring a particular value of a performance measure (Moehle and Deierlein, 2004). Under this framework, performance is computed by integrating (1) the probability of incurring an earthquake of different intensities over all possible intensities, (2) the probability of incurring a certain building response (e.g. drift, acceleration, etc.) given an intensity of ground shaking, and (3) the probability of incurring certain damage and consequences given a value of building response (FEMA, 2012). Additionally, the results were used to construct seismic vulnerability functions to permit rapid loss evaluations for regional and/or building portfolio risk assessments.

The risk-based assessments were carried out consistent with the 2014 and 2018 NSHMs. Additionally, a scenario-based assessment was performed to evaluate the response of the archetype buildings conditioned on the occurrence of the M9 CSZ simulated earthquake scenarios. At each earthquake intensity level considered in the study, two thousand Monte Carlo simulations were carried out to evaluate the earthquake-induced losses. For each realization, the losses are calculated as follows: (i) engineering demand parameters, e.g. peak story drifts and accelerations (e.g. Figure 3), are estimated from the results of nonlinear dynamic analyses; (ii) fragility functions are used in conjunction with engineering demand parameters to determine the associated damage state for each component (structural and non-structural); (iii) consequence functions are then used to translate damage states into repair costs (FEMA, 2012). The direct economic losses for each realization are then estimated by conducting this calculation for every component at every story throughout the building. The loss assessment was carried out using SP3 (SP3, 2019), a software which implements the FEMA P-58 methodology (FEMA, 2012).

A building performance model was created for each archetype building, considering variations in height and design strategy, to enable estimating its earthquake-induced repair costs. The building replacement cost for each archetype residential building was estimated assuming a cost of $230 per sq. ft. by adjusting values recommended by FEMA P-58 for office buildings in California to account for differences in location (SP3, 2019) and occupancy type (RS Means, 2019).

Structural component quantities were based on the structural design of each archetype building, with slight variations depending on the design strategy. Non-structural component quantities were estimated based on typical quantities found in residential buildings using the FEMA P-58 Normative Quantity Estimation Tool (FEMA, 2012) and adjusted per the recommendations of USGS (2018b) and ATC (2018). Non-structural quantities per story were generally consistent for all building archetypes. Table 3 provides a summary of the building performance model assumptions for all archetype buildings including the structural and non-structural components adopted, their fragility numbers (unique identifiers), component category (e.g. structure, façade, MEP, fitouts, etc.), quantity, unit, distribution of components throughout the building, and the engineering demand parameters (EDP) the fragility function were conditioned on.

Different engineering demand parameters were used for different building components, depending on their ability to predict damage (e.g., damage to acceleration-sensitive components can be estimated by peak floor accelerations). The following demand parameters, derived from the nonlinear analysis results, were used to evaluate performance of the archetype residential RC shear wall building: story drifts, residual drift, damageable wall drift, racking drift, and floor acceleration. Racking drift deformations occur in the RCSW structure due to the difference between the vertical deformation at the shear wall edges and the gravity frame columns. The racking drift causes damage and losses associated with interior partition wall finishes and slab-to-column connections. For the damage assessment of wall piers, simply using story drift ratio as a proxy for damage is not appropriate. For instance, on the upper floors of the archetype buildings, rigid body rotation contributes significantly to the story drifts. However, this mode of deformation does not cause damage to the wall piers in the upper stories. Therefore, damageable wall drifts, which remove the effect of rigid body rotation, were used as a better proxy for damage.

Residual drift was also included in the analysis to account for cases where the building is assumed to be damaged beyond repair. Residual drift is uncertain and highly sensitive to the nonlinear modeling assumptions and ground motion characteristics. Hence, residual drift was estimated as a function of peak story drift and yield drift following FEMA (2012) recommendations. A building repair fragility, represented by a cumulative lognormal distribution with a median value of 1% residual drift ratio and a dispersion of 0.3, was assumed in the analysis. Similarly, the building-specific collapse fragilities presented earlier were used to determine varying probabilities of collapse at different

ground motion shaking intensities. While the nonlinear simulation of structural response was performed using 2D models in the uncoupled direction of the RC shear wall buildings, loss estimation requires inputs in both orthogonal directions. Quantities in the uncoupled direction were considered for the coupled direction as well. As a result, demand parameters were assumed to be the same in both building directions (i.e., uncoupled and coupled).

Table 3. Structural and non-structural components per story for all archetype residential RC shear wall buildings.

Fragility ID	Component	Quantity[1]	Unit	Location	EDP
B1044.1xx[2]	Slender Concrete Wall	Varies[2]	144 SF	All Stories[3]	Damageable Wall Drift
B1049.012	RC Slab-Column Connection	12	Each	All Stories	Racking Drift
B2022201[4]	Curtain Walls	67	30 SF	Stories (TYP.)[5]	Story Drift
C1011.001a	Wall Partition w/ Metal Studs	6	100 LF	Stories (TYP.)	Racking Drift
C3011.001a	Wall Partition Finishes	1.91	100 LF	Stories (TYP.)	Racking Drift
C2011.001a	Prefabricated Steel Stair w/ Seismic Joint	2	Each	All Stories	Story Drift
D101411ridr[6]	Elevator Guide Rail System	(2 or 4)[7]	Each	Ground Level	Residual Drift
D1014.011	Traction Elevator Cabin	(2 or 4)[7]	Each	Ground Level	Acceleration
D3041.001c	HVAC Fan	0.4	10 Each	Stories (TYP.)	Acceleration
D3041.011c	HVAC Ducting	0.5	1000 LF	Stories (TYP.)	Acceleration
D5012.023b	Low Voltage Switchgear	1	225 Amp	Stories (TYP.)	Acceleration
D2022.023a	Heating Water Piping – Large Diameter	0.056	1000 LF	Stories (TYP.)	Acceleration
D2022.013a	Heating Water Piping – Small Diameter	1.55	1000 LF	Stories (TYP.)	Acceleration
D2022.023b	Heating Water Pipe Bracing – Large Diameter	0.056	1000 LF	Stories (TYP.)	Acceleration
D2022.013b	Heating Water Pipe Bracing – Small Diameter	1.55	1000 LF	Stories (TYP.)	Acceleration
D2021.023a	Potable Water Piping	0.075	1000 LF	Stories (TYP.)	Acceleration
D2021.023b	Potable Water Pipe Bracing	0.075	1000 LF	Stories (TYP.)	Acceleration
D3041.041b	Variable Air Volume Box	0.4	10 Each	Stories (TYP.)	Acceleration
D2031.023a	Sanitary Waste Piping – Piping Fragility	1.34	1000 LF	Stories (TYP.)	Acceleration
D2031.023b	Sanitary Waste Piping – Bracing Fragility	1.34	1000 LF	Stories (TYP.)	Acceleration
D4011.023a	Fire Sprinkler Water Piping	5.63 2.2	1000 LF	Basement Levels Stories (TYP.)	Acceleration
D4011.053a	Fire Sprinkler Drop	3.07 1.2	1000 LF	Basement Levels Stories (TYP.)	Acceleration
D3041.032c	HVAC Drops / Diffusers	8	10 Each	Stories (TYP.)	Acceleration
C3032.003a	Suspended Ceiling	40	250 SF	1st Floor above Ground	Acceleration
D3031.023(i or l)[8]	Cooling Tower	1	Each	Roof Only	Acceleration
D3052.013(i or l)[9]	Air Handling Unit	1	Each	Roof Only	Acceleration
D3031.013(f or i)[10]	Chiller	1	Each	Roof Only	Acceleration

[1] These quantities are relative to the unit values.
[2] Varies per archetype based on the RC core wall size and geometry.
[3] All stories include typical stories (above grade) as well as basement levels (below grade).
[4] User-defined fragility functions were defined for three damage states with the median story drift ratios of 0.01, 0.03, and 0.04 respectively. Dispersion was assumed to be equal to 0.3 for all damage states.
[5] Includes all stories above ground.
[6] User-defined fragility functions were defined for two damage states with the median elevator residual drift ratios of 0.002 and 0.005 respectively. Dispersion was assumed to be equal to 0.3 for both damage states.
[7] Two elevators for 8- and 12-story archetypes. Four elevators used for all other archetypes.
[8] D3031.023i used for 8- and 12-story archetypes. D3031.023l used for all other archetypes. The quantity and size for the cooling tower were adjusted per the building's total square footage.
[9] D3052.013i used for 8-, 12-, and 16-story archetypes. D3052.013l used for all other archetypes. The quantity and size for the air handling unit were adjusted per the building's total square footage.
[10] D3031.013f used for 8-, 12-, 16-, and 20-story archetypes. D3031.013i used for all other archetypes. The quantity and size for the cooling tower were adjusted per the building's total square footage.

INDICATORS OF SEISMIC PERFORMANCE

Simulated M9 Scenario vs 975-year and 2475-year Intensity Level Losses

For each of the seven categories of archetypes, Figure 7 shows the mean losses under the M9 earthquake, 975-yr intensity level and 2475-yr intensity levels per both the 2014 and 2018 NSHMs. As seen in Figure 7, the expected earthquake-induced repaired costs of the REF archetype buildings conditioned on the occurrence of the simulated M9 scenarios ranges from 47% to 61% of building replacement cost, depending on the number of stories. Benchmarking these metrics against probabilistic estimates of the intensity reveals that on average the M9 losses (a) lie between 975-year and 2475-year intensity levels per the 2018 NSHM, and (b) exceed the losses corresponding to the 2475-year intensity level per the 2014 NSHM. For all 8- to 24-story REF archetypes, the expected loss under the M9 simulations was on average 55% of building replacement cost, whereas the 975-year and 2475-year 2018 NSHM losses were approximately 50% and 93% of the building replacement costs, respectively.

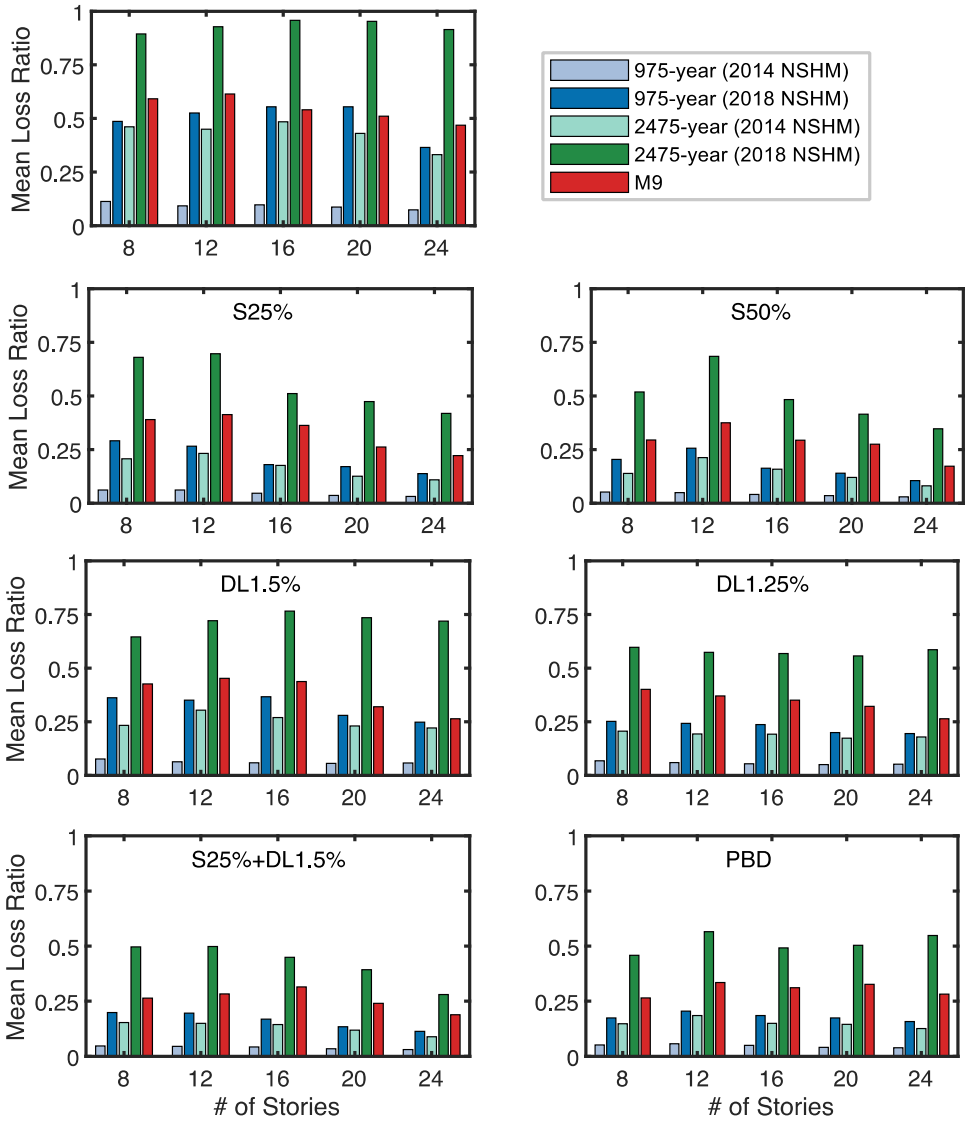

Figure 7. Mean losses under the M9 earthquake vs 975-yr and 2475-yr intensity levels per the 2014 and 2018 NSHMs.

Figure 8 illustrates the loss breakdown of the 16-story REF archetype under different hazards. As seen in the figure, the major contributor to the loss for all intensity levels is irreparable damages caused by residual drifts with the exception of the 975-year intensity level per the 2014 NSHM, which is dominated by repairable damage to structural and non-structural components. There are considerable loss contributions due to collapse for the 16-story REF archetype under the M9 simulations as well as the 2475-year intensity level per the NSHM 2018, where collapse contributions to expected loss are 13% and 28% of the total replacement cost, respectively.

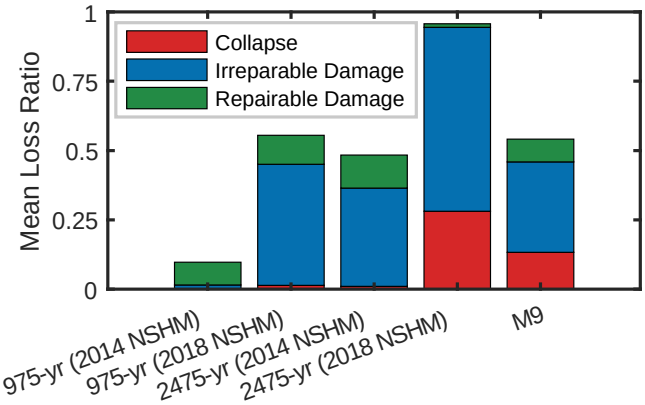

Figure 8. Mean loss breakdown for the 16-story REF archetype under the M9 earthquake vs 975-yr and 2475-yr intensity levels per the 2014 and 2018 NSHMs.

Vulnerability Functions and Annualized Earthquake-induced Repair Costs

Vulnerability functions are powerful tools to estimate expected (mean) losses at different earthquake intensity levels. In this study, expected losses were calculated for all archetype buildings, considering variations in height and design strategy. Figure 9 shows the vulnerability functions for the 16-story archetype buildings, which describes the expected loss ratio as a function of the return period of SA_{T1} per the 2014 and 2018 NSHMs. The loss ratio is equal to the expected earthquake-induced repair costs, as determined from the loss assessment, normalized by the replacement value of the building. As seen in Figure 9, at any return period, expected losses per the 2018 NSHM are considerably higher than those of the 2014 NSHM for all archetypes considered in the assessment. Furthermore, it can be observed that losses for REF archetype are considerably higher than all other design strategies considered. Considering the 16-story archetype buildings, DL1.5% is the least effective and S25%+DL1.5% is the most effective design strategy to reduce losses. For example, under the 2475-year intensity level per the 2018 NSHM, the expected loss for the DL1.5% archetype is 20% lower than the REF archetype, whereas for the S25%+DL1.5% archetype, the reduction in loss is 51%.

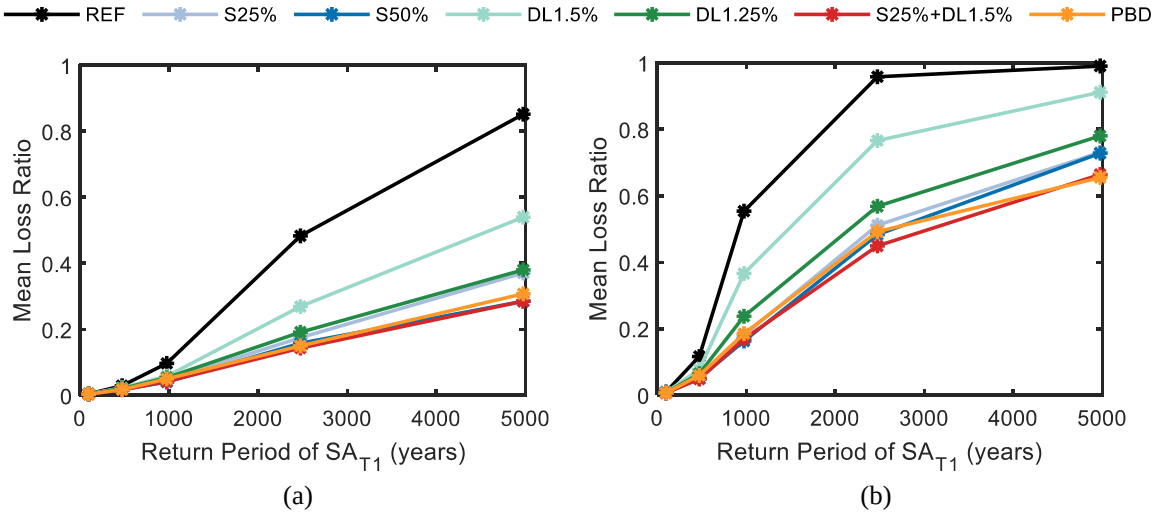

Figure 9. Loss vulnerability functions for the 16-story archetypes per (a) the 2014 and (b) the 2018 NSHMs.

Past studies suggest that many owners may elect to replace buildings when the projected repair costs exceed about 40% to 50% of the replacement cost (FEMA, 2012). When basin effects are neglected (Figure 9a), the 16-story REF archetype reaches this threshold at a return period of approximately 2500 years. Consideration of basin effects lowers the return period of this critical loss threshold to less than 1000 years. However, adopting the S25%+DL1.5% design strategy would increase the return period back to 2500 years.

While vulnerability functions provide the loss values at various earthquake intensity measure levels, average annual loss (AAL) is a useful metric to describe the anticipated economic losses considering damage at all earthquake shaking intensity levels, expressed in the form of an annualized payment, typically normalized by the building replacement cost. Hence, this metric can be regarded as a proxy for annual insurance payments. In estimating AALs, it is useful to deaggregate the loss in terms of its key contributors: (a) repairable damage, (b) irreparable damage due to excessive residual drifts (requiring demolition), and (c) collapse. Figure 10 shows the loss breakdown at different intensity levels, as well as the AAL for 16-story REF archetype per the 2014 and 2018 NSHMs. As illustrated in the figure, consideration of basin effects resulted in a threefold increase in the AAL of the 16-story REF archetype from 0.06% to 0.17% of building replacement cost, which for the archetype building considered, is equivalent to $34000 and $96000 in annual losses, respectively.

Past studies (e.g., Ramirez and Miranda, 2012; Molina Hutt et al., 2019) suggest that irreparable damage drives the AALs in modern buildings, whereas collapse drives the losses in older seismically vulnerable buildings. As illustrated in Figure 10a, the collapse contribution to AAL is low per the 2014 NSHM, highlighting the success of code provision in delivering low collapse risk (<1% in 50 years). However, consideration of basin effects resulted in a collapse risk that exceeded the code target (1% in 50 years) and consequently led to a considerable collapse contribution to AAL, 15% for the REF archetype, as seen in Figure 10b.

Figure 10 also illustrates the different loss contributions at each intensity level considered in the assessment. Regardless of the hazard model, at lower intensity levels (return period of 100 and 475 years) losses are driven by repairable damage, including structural and non-structural component damage. However, at higher intensity levels (return period greater than 2475 years per the 2014 NSHM and 975 years per the 2018 NSHM) irreparable damage due to excessive residual drift becomes the greatest contributor to the loss, with the exception of the 4975-year intensity level per the 2018 NSHM, where collapse dominated the loss.

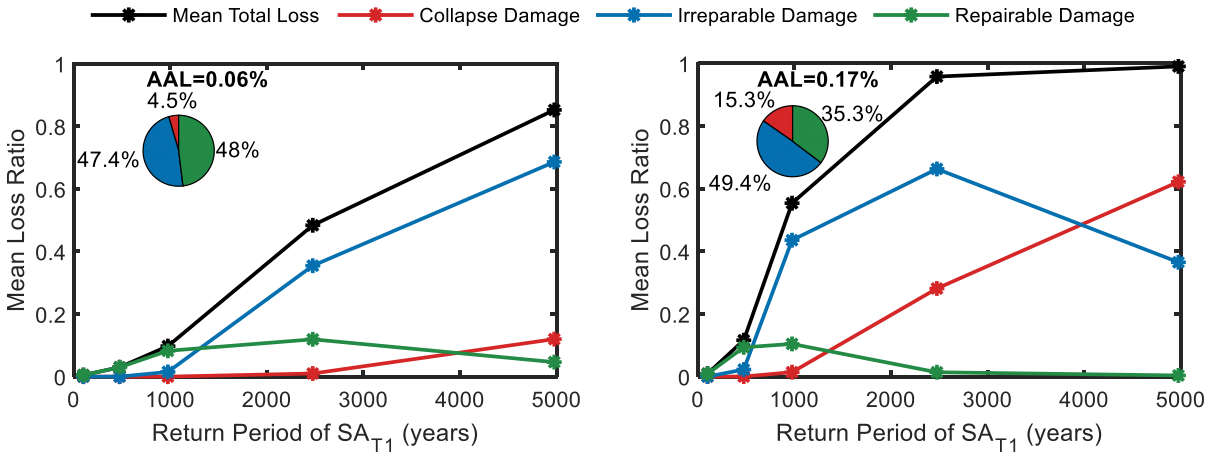

(a) (b)

Figure 10. Loss vulnerability functions and associated AAL including contributions from collapse, irreparable and repairable damage for the 16-story REF archetype per (a) the 2014 and (b) the 2018 NSHMs.

Figure 11 summarizes the AALs for the 8- to 24-story archetypes and all different design strategies, which were computed using three distinct seismic hazard models: 2014 NSHM, 2018 NSMH and 2018 NSHM+M9. The latter represents a hybrid seismic hazard model, which is based on the 2018 NSHM, but utilizes physics-based simulations to represent the large interface earthquake portion of the hazard and empirical relationships for all other earthquake

sources (crustal and intraslab). The hybrid seismic hazard model permits calculating AALs as outlined in Equation (1).

$$AAL_{NSHM\ 2018+M9} = AAL_{NSHM\ 2018} - AAL_{Interface} + AAL_{M9} \quad (1)$$

where, $AAL_{NSHM\ 2018+M9}$ is the total seismic loss per the 2018 NSHM with the M9 simulations representing interface earthquake contribution to the hazard, $AAL_{NSHM\ 2018}$ is the seismic loss per the 2018 NSHM, $AAL_{Interface}$ is the seismic loss associated with interface earthquakes only, and AAL_{M9} is the seismic loss corresponding to the M9 simulations.

Figure 11 illustrates that the 2018 NSHM, i.e. considering basin effects, resulted in approximately a threefold increase in AALs over the 2014 NSHM for all archetypes. Furthermore, using physics-based simulations to represent the large interface earthquake portion of the hazard further amplified the losses relative to the 2018 NSHM. It should be noted that the average increase of AAL of the hybrid model over the 2018 NSHM was around 28% for the 8-, 12-, and 16-story archetypes, where the increase in 16-story archetypes was slightly higher than the 8- and 12-story archetypes. However, the increase dropped to 24% for the 20-story archetypes and 16% for the 24-story archetypes.

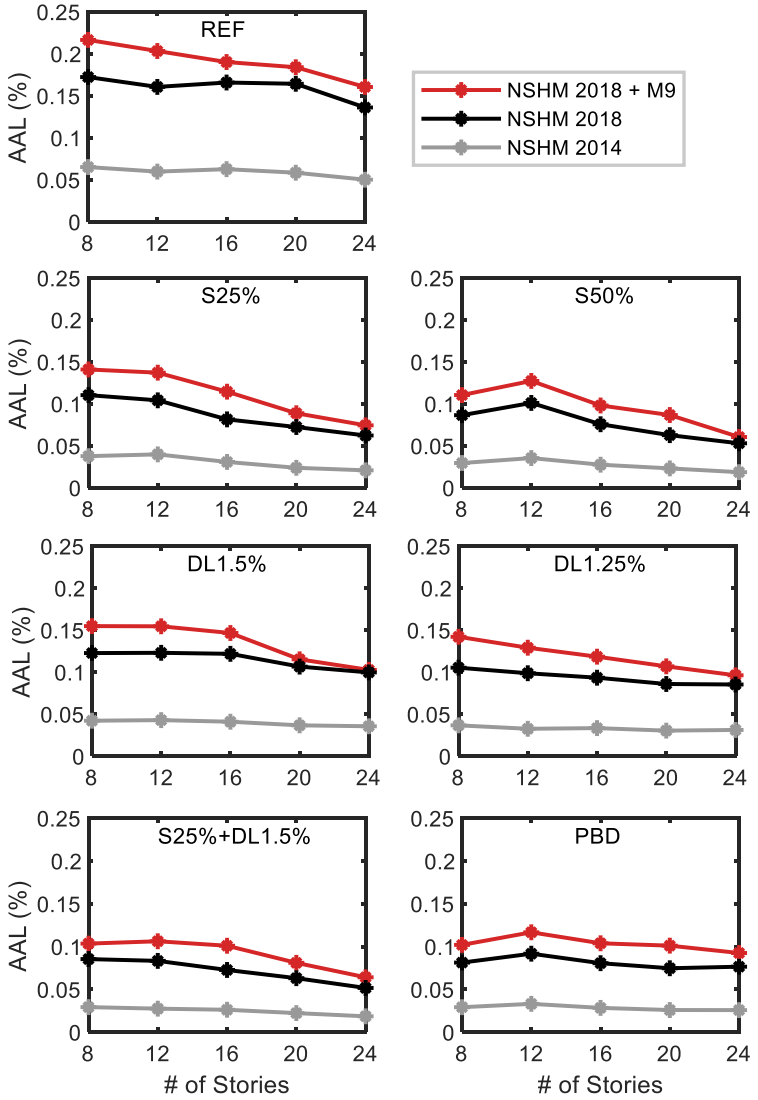

Figure 11. AALs for the 8- to 24-story archetypes, all different design strategies and all seismic hazard models.

Figure 12 compares the impact of the different design strategies on the average annual loss for the hybrid seismic hazard. The results suggest that S25%+DL1.5% was the most effective and DL1.5% was the least effective strategy, achieving an average 53% and 30% reduction in loss respectively, over the REF archetypes. Figure 12 also suggests that increasing design strength was a more efficient strategy to reduce earthquake-induced economic losses compared to increasing stiffness.

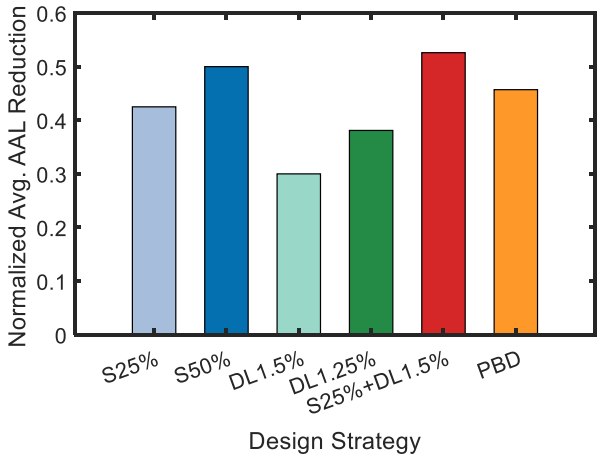

Figure 12. AAL change of enhanced archetypes relative to REF archetype per the hybrid seismic model (average for all archetype stories).

Relationship between Annualized Loss and Annualized Collapse Risk

In order to study the relationship between annualized losses and collapse risk, the annualized collapse risk (λ_c) of each archetype was computed following a similar procedure that was used to calculate AAL, by combining its collapse fragility, expressed in terms of SA_{T1}, with the seismic hazard curve. Collapse risk was only calculated per the 2018 NSHM, because collapse probabilities per the 2014 NSHM were negligible. Figure 13 illustrates the relationship between AAL and λ_c under the 2018 NSHM.

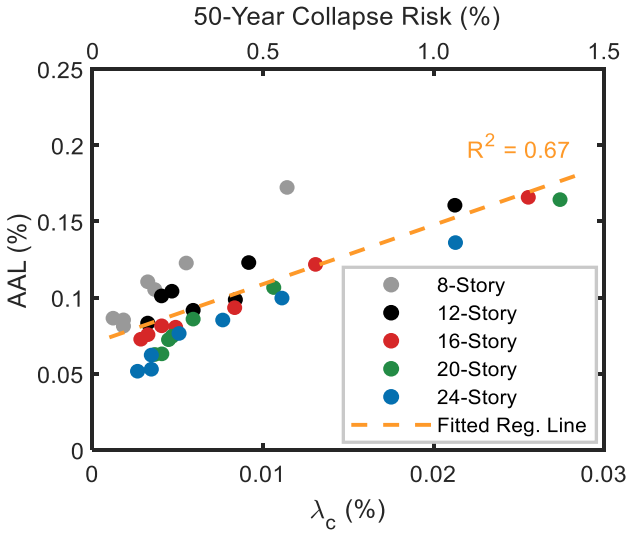

Figure 13. Relationship between AAL and λ_c per the 2018 NSHM.

50-year collapse risk is calculated assuming collapse occurrence follows the Poisson distribution, which provides a benchmark against the maximum of 1% in 50 year targeted by ASCE 7-16. There is a strong linear correlation between AAL and λ_c for all archetypes with R-squared values of over 0.95 for the 8-, 16-, 20-, and 24-story archetypes and around 0.9 for the 12-story buildings. This indicates that buildings with higher collapse risk tend to have higher

earthquake-induced annual losses. While the slope of the regressed line is similar for all archetypes ranging from 12- to 24- stories, it is different for the 8-story archetypes, which are the only height for which the REF design complies with the code collapse-risk target of less than 1% in 50 years. If all archetypes from 8- to 24- story archetypes were grouped as a single set of data points, there would still be a correlation between AAL and λ_c for the new dataset, with an R-squared value of 0.67. These results suggest that the AAL for modern RC-shear wall building within the range of 8- to 24- stories can be estimated from the λ_c using Equation (2).

$$AAL_{8\text{-to }24\text{-stories}} = 3.8836\,\lambda_c + 0.0007 \quad (2)$$

On the other hand, if 12- to 24-story archetypes were grouped as a single set of data points, the correlation between AAL and λ_c will be stronger, resulting in a R-squared value of 0.85.

CONCLUSIONS

This study quantified the earthquake-induced economic losses of a series of modern 8- to 24-story residential RC shear wall building archetypes in Seattle, with and without consideration of basin effects, as implemented in the 2018 and the 2014 NSHMs, respectively. In addition, a hybrid hazard model was considered in the loss assessment to incorporate recent M9 CSZ earthquake simulations to represent the large contribution to the hazard of interface seismic sources. Expected losses were calculated at a variety of intensity levels for all archetype buildings. Losses were then integrated with the corresponding seismic hazard curves to report average annual losses (AALs). Finally, losses were computed for different archetype design strategies. The summary of findings for this study is as follows:

- Losses under the simulated M9 CSZ earthquakes (with a return period of about 500 years) were bounded by the 2018 NSHM 975-year and 2475-year intensity level losses. On average, the expected loss under the M9 simulations was 55% of building replacement cost across all REF archetypes, whereas the 975-year and 2475-year losses were around 50% and 93% of the building replacement costs, respectively.
- Consideration of basin effects within the probabilistic seismic hazard assessment (i.e., 2018 NSHM vs 2014 NSHM) resulted in a threefold increase in AALs for a wide range of story heights.
- Consideration of physics-based simulations in the loss assessment resulted in a further increase of 22% on average over the 2018 NSHM estimates. The minimum increase of 16% was observed in the 24-story archetypes, and the maximum increase of 28% was observed in the 16-story archetypes.
- Comparison of AALs across all design schemes considered per the hybrid hazard model revealed that the S25%+DL1.5% (an increase in design forces by 25%, coupled with a reduction in drift limits to 1.5%) was the most effective and DL1.5% (reducing drift limits from 2% to 1.5%) was the least effective strategy to reduce annual losses relative to REF archetypes, achieving an average of 53% and 30% reduction in losses, respectively.
- The PBD designs provide an economic solution in terms of material costs, which are lower than the S25%+DL1.5% design scheme, and seismic losses, which are slightly higher than the S25%+DL1.5% design scheme. However, PBD designs bare a higher engineering cost, as they require non-linear analysis to check inelastic strains, drifts, and forces, and involve a detailed peer review process. While these higher engineering cost implications are not considered in this study, if material savings outweigh design premiums, PBD provides a good solution.
- There was a strong correlation between AAL and the annualized collapse risk, λ_c for all archetypes. The trends were very similar for all, but the 8-story archetypes due to smaller collapse risks compared to all others. However, AALs could still be inferred from λ_c for modern 8- to 24-story RC shear wall buildings using a fitted regressed line with a R-squared value of 0.67.

ACKNOWLEDGEMENTS

This research was funded by Canada's Natural Sciences and Engineering Research Council under Discovery Grant No. RGPIN-2019-04599, as well as Canada's New Frontiers in Research Fund – Exploration under Grant No. NFRFE-2018-01060. The authors would also like to thank the University of British Columbia's Cascadia Engagement Fund for supporting this collaboration with the University of Washington. The computations were facilitated by HB Risk, who provided access to their Seismic Performance Prediction Program (SP3). Support was also provided by the U.S. National Science Foundation under Grant No. EAR-1331412 and by the United States Geological Survey Earthquake Hazards Program under grant G19AP00049. Any opinion, findings, and conclusions or recommendations expressed

in this material are those of the authors and do not necessarily reflect the views of the collaborators or sponsoring agencies.

REFERENCES

Aagaard BT, Graves RW, Rodgers A, et al. Ground-motion modeling of Hayward fault scenario earthquakes, part II: Simulation of long-period and broadband ground motions. *Bull Seismol Soc Am*. 2010;100(6):2945–2977.

Abrahamson N, Gregor N, Addo K. BC hydro ground motion prediction equations for subduction earthquakes. *Earthq Spectra*. 2016;32(1):23–44.

ACI. *Building code requirements for structural concrete and commentary, ACI 318-14*. American Concrete Institute, Farmington Hills, MI. 2014.

ASCE. *Minimum design loads for buildings and other structures, ASCE/SEI 7-16*. American Society of Civil Engineers, Reston, VA. 2016.

ATC. *San Francisco tall buildings study*, Applied Technology Council, Redwood City, CA. 2018.

Baker JW. Efficient analytical fragility function fitting using dynamic structural analysis. *Earthq Spectra*. 2015;31(1):579–599.

Baradaran Shoraka M, Yang TY, Elwood KJ. Seismic loss estimation of non-ductile reinforced concrete buildings. *Earthquake Engng Struct Dyn.* 2013;42:297–310.

Bozorgnia Y, Abrahamson NA, Atik L, et al. NGA-West2 research project. *Earthq Spectra.* 2014;30(3):973–987.

Choi Y, Stewart JP, Graves RW. Empirical model for basin effects accounts for basin depth and source location. *Bull Seismol Soc Am.* 2005;95(4):1412–1427.

City of Seattle Department of Planning and Developments. Alternate design requirements for use of special reinforced concrete shear walls in over height buildings. Retrieved April 21, 2018, from www.seattle.gov/dpd/codes/dr/DR2015-5.pdf. 2015.

Dilger WG, Brown SJ. Earthquake resistance of slab-column connection. In festschrift Professor Dr. Hugo Bachmann Zum, 22–27. ETH Zurich, Switzerland. 1995.

Dilger WG, Cao H. Behaviour of slab-column connections under reversed cyclic loading. Proceedings 2nd International Conference of High-Rise Buildings 1991; Beijing, China: Atlantis Press.

Eberhard MO, Meigs BE. Earthquake-Resisting System Selection Statistics for Reinforced Concrete Buildings. *Earthq Spectra*. 1995;11(1):19–36.

FEMA. *Seismic performance assessment of buildings FEMA P-58*, Federal Emergency Management Agency, Washington, DC. 2012.

Frankel A. Modeling strong-motion recordings of the 2010 M_w 8.8 Maule, Chile, earthquake with high stress-drop subevents and background slip. *Bull Seismol Soc Am*. 2017;107(1):372–386.

Frankel A. Rupture history of the 2011 M9 Tohoku Japan earthquake determined from strong-motion and high-rate GPS recordings: Subevents radiating energy in different frequency bands. *Bull Seismol Soc Am*. 2013; 103(2B):1290–1306.

Frankel A, Wirth E, Marafi N, et al. Broadband synthetic seismograms for magnitude 9 earthquakes on the Cascadia megathrust based on 3D simulations and stochastic synthetics, Part 1: Methodology and overall results. *Bull Seismol Soc Am*. 2018;108(5A):2347–2369.

Goretti A, Molina Hutt C, Hedelung L. Post-Earthquake safety evaluation of buildings in Portoviejo, Manabí following the M7.8 coastal Ecuador earthquake of 16 April 2016. *Int J Disaster Risk Reduction*. 2017;24:271–283.

Graves R, Jordan TH, Callaghan S, et al. CyberShake: A physics-based seismic hazard model for southern California. *Pure Appl Geophys*. 2011;168(3-4):367–381.

Hueste MBD, Browning JA, Lepage A, et al. Seismic design criteria for slab-column connections. *ACI Struct J.* 2007;104(4):448–458.

Hueste MBD, Kang THK, Robertson IN. Lateral drift limits for structural concrete slab-column connections, including shear reinforcement effects. Proceedings ASCE Structures Congress 2009; Austin, TX.

Hwang SH, Lignos DG. Earthquake-induced loss assessment of steel frame buildings with special moment frames designed in highly seismic regions. *Earthquake Engng Struct Dyn*. 2017;46:2141–2162.

Jalayer F, Cornell CA. Alternative non-linear demand estimation methods for probability-based seismic assessments. *Earthquake Engng Struct Dyn.* 2009;38(8):951–972.

Jayaram N, Lin T, Baker JW. A Computationally efficient ground-motion selection algorithm for matching a target response spectrum mean and variance. *Earthq Spectra.* 2011;27(3):797–815.

Ji X, Liu D, Ya S, et al. Seismic performance assessment of a hybrid coupled wall system with replaceable steel coupling beams versus traditional RC coupling beams. *Earthquake Engng Struct Dyn.* 2017;46:517–535.

Ji X, Liu D, Molina Hutt C. Seismic performance evaluation of a high-rise building with novel hybrid coupled walls. *Eng Struct*. 2018;169:216–225.

Kunnath SK, Heo Y and Mohle JF. Nonlinear uniaxial material model for reinforcing steel bars. *J Struct Eng*. 2009;135(4):335–343.

Marafi NA, Ahmed KA, Lehman DE, et al. Variability in seismic collapse probabilities of solid- and coupled-wall buildings. *J Struct Eng.* 2019a;145:1–17.

Marafi NA, Eberhard MO, Berman JW, et al. Effects of deep basins on structural collapse during large subduction earthquakes. *Earthq Spectra.* 2017;33(3):963–997.

Marafi NA, Eberhard MO, Berman JW, et al. Impacts of simulated M9 Cascadia subduction zone motions on idealized systems. *Earthq Spectra.* 2019b;35(3):1261–1287.

Marafi NA, Makdisi AJ, Berman JW, et al. Design strategies to achieve target collapse risks for reinforced concrete wall buildings in sedimentary basins. *Earthq Spectra*. 2020a, In press. https://doi.org/10.1177/8755293019899965.

Marafi NA, Makdisi AJ, Eberhard MO, et al. Impacts of an M9 Cascadia subduction zone earthquake and Seattle basin on performance of RC core-wall buildings. *J Struct Eng.* 2020b;146(2): 04019201.

McKenna F, *OpenSees*, Pacific Earthquake Engineering Research Center, University of California, Berkeley, CA. 2016.

Megally S, Ghali A. Punching shear design of earthquake-resistant slab column connections. *ACI Struct J.* 2000;97(5):720–730.

Menegotto M, Pinto PE. Method of analysis for cyclically loaded reinforced concrete plane frames including changes in geometry and non-elastic behavior of elements under combined normal force and bending. Proceedings, Symp. on the Resistance and Ultimate Deformability of Structures Acted on by Well Defined Repeated Loads, 15–22. International Association for Bridge and Structural Engineering. 1973; Zurich, Switzerland.

Moehle J, Deierlein GG. A framework methodology for performance-based earthquake engineering. Proceedings 13th World Conference on Earthquake Engineering 2004; Vancouver, Canada.

Molina Hutt C, Almufti I, Willford M, et al. Seismic loss and downtime assessment of existing tall steel-framed buildings and strategies for increased resilience. *J Struct Eng.* 2016;142(8):C4015005.

Molina Hutt C, Rossetto T, Deierlein GG. Comparative risk-based seismic assessment of 1970s vs modern tall steel moment frames. *J Constr Steel Res.* 2019;159:598–610.

Molina Hutt C, Zahedimazandarani S, Marafi NA, et al. Collapse risk of tall steel moment-resisting frames in deep sedimentary basins during large magnitude subduction earthquakes. *Eng Struct.* 2020, In review.

Morikawa N, Fujiwara H. A new ground motion prediction equation for Japan applicable up to M9 mega-earthquake. *J Disaster Res.* 2013;8(5):877–888.

Moschetti MP, Hartzell S, Ramírez-Guzmán L, et al. 3D ground-motion simulations of M_w 7 earthquakes on the Salt Lake City segment of the wasatch fault zone: Variability of long-period ($T \geq 1$ s) ground motions and sensitivity to kinematic rupture parameters. Bull Seismol Soc Am. 2017;107(4):1704–1723.

NEHRP. *Selecting and scaling earthquake ground motions for performing response history analyses NIST GCR 11-917-15*, NEHRP Consultants Joint Venture for the National Institute of Standards and Technology, Gaithersburg, MD. 2011.

PEER. *Guidelines for performance-based seismic design of tall buildings*, Report No. 2017/06. Pacific Earthquake Engineering Research Center, University of California, Berkeley, CA. 2017.

Petersen MD, Moschetti MP, Powers PM, et al. *Documentation for the 2014 update of the United States national seismic hazard maps*. U.S. Geological Survey, Reston, VA. 2014.

Petersen MD, Shumway AM, Powers PM, et al. The 2018 update of the US national seismic hazard model: Overview of model and implications. *Earthq Spectra*. 2020;36(1):5–41.

Popovics S. A numerical approach to the complete stress-strain curve of concrete. *Cement Conc Res*. 1973;3(5):583–599.

Ramirez CM, Liel AB, Mitrani-reiser J, et al. Expected earthquake damage and repair costs in reinforced concrete frame buildings. *Earthquake Engng Struct Dyn*. 2012;41:1455–1475.

Ramirez CM, Miranda E. Significance of residual drifts in building earthquake loss estimation. *Earthquake Engng Struct Dyn*. 2012;41:1477–1493.

RS Means. Building construction cost data R.S. Means Company, Kingston, MA. 2019.

SEAW earthquake Engineering committee, Personal communication, 2018.

SP3. Seismic Performance Prediction Program [Computer Software], Haselton Baker Risk Group, Chico, CA. 2019.

Stephenson WJ, Reitman NG, Angster SJ. *P- and S-wave velocity models incorporating the Cascadia subduction zone for 3D earthquake ground motion simulations, Version 1.6—Update for open-file report 2007–1348*. U.S. Geological Survey, Reston, VA. 2017.

USGS. *National Seismic Hazard Mapping Project (NSHMP) code*, U.S. Geological Survey. Reston, VA. 2019.

USGS. *Preliminary 2018 update of the U.S. national seismic hazard model: Overview of model, changes, and implications*. U.S. Geological Survey, Reston, VA. 2018a.

USGS. *The HayWired earthquake scenario. Engineering implications, United States geological survey scientific investigations report 2017-5013-I-Q*, U.S. Geological Survey, Reston, VA. 2018b.

Wirth EA, Chang SW, Frankel AD. *2018 report on incorporating sedimentary basin response into the design of tall buildings in Seattle, Washington: Open-file rep 2018–1149*, U.S. Geological Survey, Reston, VA. 2018.

Yassin MH. *Nonlinear analysis of prestressed concrete structures under monotonic and cycling loads*. University of California, Berkeley, CA. 1994.